Korean J. Chem. Eng., **29**(2), 162-168 (2012)
DOI: 10.1007/s11814-011-0198-y

Transport analysis in reverse electrodialysis with pulsatile flows for enhanced power generation

Kwang Seok Kim*, Won Ryoo, Myung-Suk Chun*,†, Gui-Yung Chung**, and Seung Oh Lee*****

*Complex Fluids Laboratory, National Agenda Res. Division, Korea Institute of Science and Technology (KIST), Seongbuk-gu, Seoul 136-791, Korea
**Department of Chemical Engineering, Hong-Ik University, Mapo-gu, Seoul 121-791, Korea
***School of Urban and Civil Engineering, Hong-Ik University, Mapo-gu, Seoul 121-791, Korea
(*Received 16 June 2011 • accepted 2 August 2011*)

Abstract−Time-dependent velocity profile and concentration distributions formed in a single reverse electrodialysis (RED) unit have been successfully pursued using simulation framework for evaluating performance of the unit, i.e., open circuit voltage and short circuit current. The single RED unit consists of two adjunct fluid channels, separated by the semi-permeable membrane. Through one of the channels, sea water flows, and the other is occupied by fresh water, flowing in the opposite direction (countercurrent operation). The diffusion-convection transport of the rate-limiting ion, Na^+ in this study, for both channels is treated. The diffusive transport of cation across the membrane is expressed as boundary conditions for the bi-mechanism model. Our simulations conducted using an orthogonal collocation on finite element scheme show that the concentration difference of 35 g/L between sea water and fresh water results in the open circuit voltage of 63 mV and the short circuit current density of 11.5 A/m^2. These values are close to ones that were obtained from the experiments.

Key words: Reverse Electrodialysis, Convection-Diffusion, Pulsatile Flow, Nernst-Planck Equation, Open Circuit

INTRODUCTION

Renewable energy has been of particular interest to scientists and engineers across the world for human survival after the age of fossil fuel. Despite its high efficiency, inherent weather-dependent power output of solar panels requires development of alternative devices that can stably harvest renewable energy. Recently, power generation using difference in ion concentrations between sea water and fresh water has been spotlighted. This was first suggested and named as reverse electrodialysis (RED) by Pattle [1,2]. RED is a reverse operation of desalination [3,4], that is, mixing fresh water with sea water slowly and orderly through semi-permeable membrane, as presented in Fig. 1. Note that mixing the two disorderly (by stirring, for example) results in no net current. It is known that the theoretical (or maximum) energy obtainable by mixing one liter of sea water with the same amount of fresh water is 0.286 Whr [5]. This means tremendous amount of sea and fresh water is required for industrial application of an RED battery. As a result, the RED power generating facility is usually installed near an estuary where both sea water and fresh water can be readily supplied. This technology can overcome the disadvantages of the solar cell or bio-diesel: salinity of sea water remains (almost) constant, which warrants stable power generation regardless of weather change; minimum (or no) opportunity cost (e.g., ecosystem disturbance) occurs.

Particularly in South Korea, annually around 38.6 billion tons of fresh water is flowing out to sea. This amount of fresh water is equivalent to 245 GWhr. When it is compared to 88 GWhr that is the total electric energy generated from renewable sources in 2007, RED power generating shows a promising future even though only 10% of the energy can be recovered in practice. Despite the unique advantages and potential, incarnation of the RED power generating concept still includes challengeable issues, such as high installation cost (about $8/kWhr) [6] and insufficient fundamental investigations for stable operations. To reduce the cost and to maximize the productivity, comprehensive analysis on every part in the plant is required.

Above all, solid knowledge on underlying theories of a single RED unit is a prerequisite since determination of the performance, the installation, and maintenance costs of the power plant are majorly based on the unit. For example, performance estimation of an RED unit should be based on the Nernst-Planck (N-P) principle [6,7], which states that the ionic flux is the result of combined mecha-

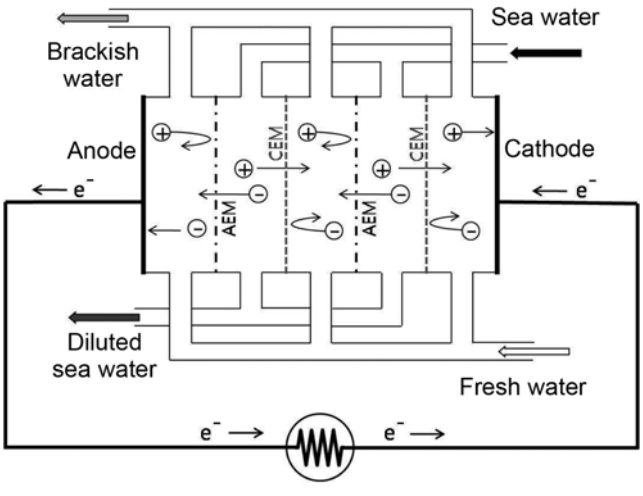

Fig. 1. Schematic drawing of an RED generator.

†To whom correspondence should be addressed.
E-mail: mschun@kist.re.kr

nisms such as convection, diffusion, and migration. The present study is carried out using a model for convection-diffusion transport of ion and computer simulations aimed at an inside-view of flow pattern, ion distribution and subsequently electrical properties of a single unit. Particularly, effect of pulsatile flows, introduced for both sea and fresh water streams, on the performance of RED was emphasized. An industrial RED power plant consists of multiple units stacked and peripheral devices (Fig. 1). In line with those assignments, the rest of this paper was written so as to contribute to the particular tasks including schematic notation of RED cells, convection-diffusion model of ion species for each cell, computer simulation results, and open circuit voltage and short circuit current of a single unit.

MODEL DEVELOPMENT

1. Single RED Unit

Before getting into details, visual aids shown in Fig. 2, respectively, demonstrate the key transport mechanisms that take place in a single RED unit and the selection of the rectangular coordinates for the analysis. The entire RED system consists of two types of membranes (thickness of W_M), parallel to one another, separated by B, and placed in an alternating order. The gaps formed by the membranes are occupied by sea and fresh water streams also in an alternating order. Fig. 2(a) represents a single unit out of the repeating ones. The membrane placed in the middle (the space between dashed lines) is semi-permeable to Na^+, while the membranes on either side (outer regions of each bold line) are to Cl^-. The sea water stream loses Na^+ ion to the right cell and Cl^- ions to the left cell (diffusive transport), staying neutral. Now that the diffusive transport of Na^+ is known much slower than that of Cl^-, the analysis only on Na^+ transport is able, in sufficient accuracy, to represent the behavior of the entire system. This means that the Cl^- transport through the other membrane will take place as the same amount of the Na^+ transport [8]. Both streams are countercurrent (convective transport) to each other, known to be helpful keeping driving force highest. Within the membrane, it is assumed that there is no convective flow due to relatively confined channels.

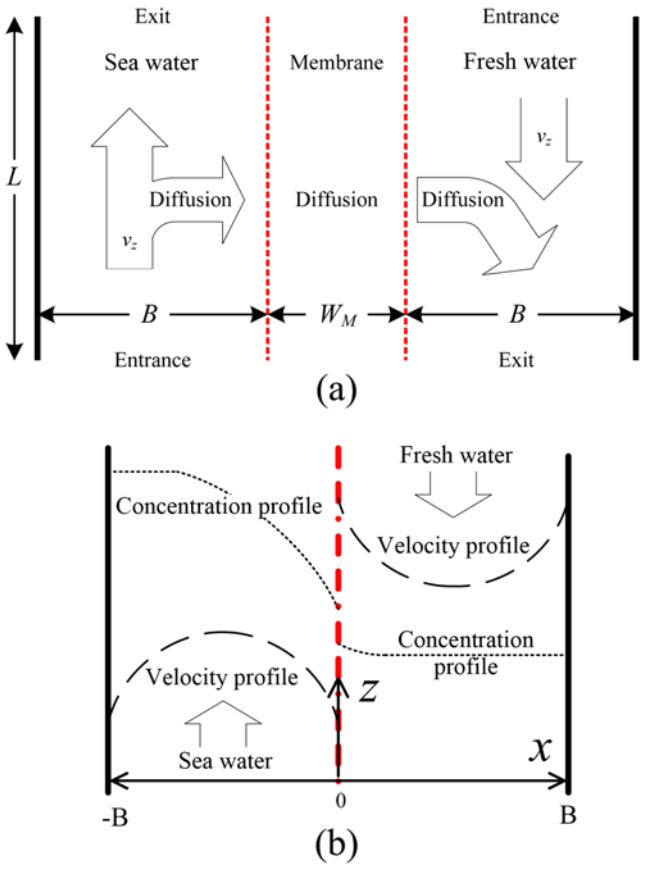

Fig. 2. Two-dimensional transport mechanisms in (a) single RED unit, and (b) selected coordinates system for analysis.

By the way, the coordinate system in Fig. 2(b) does not take the existence of the membrane into consideration. In fact, the transport of the ion, only by diffusion, through the membrane (denoted by a double-dash-dot line at the center) can be readily substituted into boundary conditions. This will be addressed in the following section. Figs. 2(a) and 2(b) are not drawn to scale. In fact, width and length of each wall are much greater than the gap (=B). In this occasion, flowing through a slit without end effect can be employed for analysis.

2. Ion Transport Across RED Cells

The governing equation for each concentration profile c_i in both slit-like channels can be derived from the conservation of species based on the convection-diffusion. In the rectangular coordinate, it is expressed as

$$\frac{\partial c_i}{\partial t} = D_i \frac{\partial^2 c_i}{\partial x^2} - v_i \frac{\partial c_i}{\partial z} \tag{1}$$

where D_i is diffusion coefficient of Na^+ in aqueous solution provided by Fick's law, and v_i denotes the velocity of water. Precisely, diffusivity is a function of concentration, even though it may be weak. The subscript i indentifies each stream, which corresponds to H and L for sea water and fresh water streams, respectively. In Fig. 2, the sea water of concentration c_0 enters the cell at z=0 and the fresh water does at z=L, which corresponds to the boundary conditions:

$$c_H|_{z=0} = c_0, \tag{2}$$

$$c_L|_{z=L} = 0. \tag{3}$$

No flux of Na^+ is allowed through the membranes at x=±B. Consequently, this leads to the following boundary conditions:

$$\left.\frac{\partial c_H}{\partial x}\right|_{x=-B} = 0, \tag{4}$$

$$\left.\frac{\partial c_L}{\partial x}\right|_{x=B} = 0. \tag{5}$$

At the interfaces formed with the membrane favorable for Na^+ and liquid in both cells, the assumption of fast equilibrium in concentrations leads to the following boundary conditions:

$$c_H|_{x=0^-} = K_H c_M|_{x=0^-}, \tag{6}$$

$$c_L|_{x=0^+} = K_L c_M|_{x=0^-}, \tag{7}$$

where K_H and K_L are the partition coefficients [9] of the sea and

the fresh water, respectively.

3. Time-dependent Convection

The pressure-driven velocity field for an incompressible Newtonian aqueous fluid at the steady state obeys the Navier-Stokes (N-S) equation of motion [7] such that

$$\rho\frac{\partial v_i}{\partial t}=-\frac{\Delta p}{L}+\mu\frac{\partial^2 v_i}{\partial x^2}, \tag{8}$$

where ρ and μ are the density and viscosity of fluid, respectively. In Eq. (8), effect of inertia, which was supposed to be shown on the left-hand side, is readily ignored because it is widely known that a low Reynolds number flow system is commonly employed in the RED cell. At each surface of the membranes, Eq. (8) is subjected to the non-slip boundary conditions such that

$$v_i=0 \qquad \text{at } x=0 \text{ or } \pm B. \tag{9}$$

Based on the time-periodic function for the unidirectional pulsatile flow, the pressure gradient is given in the form of sinusoidal wave [10], such that

$$\Delta p=\begin{cases}-\dfrac{p_{max}}{2}[1-\cos(2\pi ft)] & \text{if } x<0,\\ \dfrac{p_{max}}{2}[1-\cos(2\pi ft)] & \text{if } x>0.\end{cases} \tag{10}$$

Here, f is frequency (in Hz) and the subscript "max" denotes the maximum value. Depending on the frequency, fluid entering a channel may or may not undergo flow and pause repeatedly before it leaves the channel, in which it repeats many times for high frequency. The steady flow is a specific case of the time-dependent problem where the frequency approaches zero. Therefore, there is no pause, and the fluid flows at the average pressure gradient of $p_{max}/2$. The frequency is set reciprocal to the mean residence time, meaning the average velocity divided by the channel length. In this setup, the entire liquid in the RED unit is supposed to be replenished every cycle.

The average velocity v_m comes from the Hagen-Poiseuille equation [7], and its solution for the steady pressure case of Eqs. (8) and (9) becomes such that

$$v_m=\frac{p_{max}B^2}{24\mu L}. \tag{11}$$

By definition, the frequency f is given as

$$f=\frac{v_m}{L}=\frac{p_{max}B^2}{24\mu L^2}. \tag{12}$$

Note that we assume laminar flow. Even though the turbulence and subsequent mixing of fluid across a slit may or may not bring about in an actual unit and are known to be much beneficial, it is beyond the scope of this study.

4. Transport Across the Membrane

The last discussion in this section is about the ion transport of semi-impermeable membrane. Across the membrane, convection does not exist so that only diffusion rules out the ion transportation:

$$\frac{\partial c_M}{\partial t}=D_M\frac{\partial^2 c_M}{\partial x^2}, \tag{13}$$

where the subscript M stands for the quantity in membrane. The analytical solution of Eq. (13) can be readily found in the form of linear equation such that

$$c_M=\left(\frac{c_L|_{x=0^+}}{W_M K_L}-\frac{c_H|_{x=0^-}}{W_M K_H}\right)x+\frac{c_H|_{x=0^-}}{K_H}, \tag{14}$$

where W_M is the thickness of the membrane. Note that 0^+ and 0^- are used to denote the membrane-fresh water interface and the membrane-sea water interface, respectively. In the next section, the rationale for neglecting the membrane thickness will be addressed. In the meantime, it is postulated that the two interfaces are separated physically by W_M, but mathematically by 0. The superscripts, + or −, can be omitted when and where possible. Without such a postulate, one may have to deal with series of equations, which causes unnecessary complexity.

Considering flux conservations at both boundaries of the membrane, the following equations hold:

$$D_H\frac{\partial c_H}{\partial x}\bigg|_{x=0^-}=D_M\frac{\partial c_M}{\partial x}\bigg|_{x=0^+}, \tag{15}$$

$$D_M\frac{\partial c_M}{\partial x}\bigg|_{x=0^-}=D_L\frac{\partial c_L}{\partial x}\bigg|_{x=0^+}. \tag{16}$$

According to Eq. (14), the right-hand side of Eq. (15) and the left-hand side of Eq. (16) are equal and constant, and the rearrangement of them results in the following boundary condition:

$$D_H\frac{\partial c_H}{\partial x}\bigg|_{x=0}=D_L\frac{\partial c_L}{\partial x}\bigg|_{x=0}. \tag{17}$$

It is also noted that substitution of Eq. (14) into Eq. (15) with the assumption that $K_H=K_L$ leads to

$$D_H\frac{\partial c_H}{\partial x}\bigg|_{x=0}=\frac{D_M}{W_M K_H}(c_L|_{x=0}-c_H|_{x=0}), \tag{18}$$

or, in other form,

$$c_L|_{x=0}=c_H|_{x=0}+\left(\frac{K_H D_H}{D_M/W_M}\right)\frac{\partial c_H}{\partial x}\bigg|_{x=0}. \tag{19}$$

Collecting the necessary equations to represent the transport of ion in a single RED unit, i.e., Eqs. (1)-(5), (17), and (19), any single variable regarding the membrane is found. As a result, the existence of the semi-permeable membrane can be ignored when the numerical solution of the current problem is pursued.

Short circuit current i_{SC} and open circuit voltage Φ_{OC} are commonly measured quantities for assessing the performance of microbattery such as solar cell. In this RED cell, they are respectively estimated by

$$i_{SC}=-\frac{FD_M}{W_M}\int_A \Delta c\,dA, \tag{20}$$

$$\Phi_{OC}=\alpha\frac{RT}{\Lambda F}\ln\left(\frac{c_H}{c_L}\right), \tag{21}$$

on the basis of the N-P principle [6,7]. Here, F is the Faraday constant (96,485 C/mol), A is the area of membrane, α is the permselectivity, Λ is the valence of ion (e.g., +1 for Na^+), R is the gas con-

stant, and T is the absolute temperature in K.

5. Equations in Dimensionless Form

As many engineering applications do, an equation given in the dimensionless form can deliver plentiful convenience not only in finding a solution but also in communicating effectively with colleagues. For instance, a dimensionless parameter, a group of related dimensional quantities, facilitates rough behavioral estimation for a system of interest, even before a solution is available. This principle also applies to the analysis on the current RED cell. With dimensionless variables $C_H=c_H/c_0$, $C_L=c_L/c_0$, $X=x/B$, $Z=z/L$, $\tau=v_m t/L$, $V_i=v_i/v_m$, $Re=\rho v_m B/\mu$, $\Gamma=(D_i/B^2)/(v_m/L)$, $\delta=D_L/D_H$, and $\beta=(K_H D_H/B)/(D_M/W_M)$, the following equations can be obtained

$$\frac{\partial C_i}{\partial \tau}=\Gamma\frac{\partial^2 C_i}{\partial X^2}-V_i\frac{\partial C_i}{\partial Z}, \tag{22}$$

$$\frac{\partial V_i}{\partial \tau}=\frac{(L/B)}{Re}\left\{12(-\Delta P)+\frac{\partial^2 V_i}{\partial X^2}\right\}, \tag{23}$$

$$C_H=1 \quad \text{at } Z=0; \quad C_L=0 \quad \text{at } Z=1, \tag{24}$$

$$\left.\frac{\partial C_H}{\partial X}\right|_{X=0}=\delta\left.\frac{\partial C_L}{\partial X}\right|_{X=0}, \tag{25}$$

$$C_L|_{X=0}=C_H|_{X=0}+\beta\left.\frac{\partial C_H}{\partial X}\right|_{X=0}, \tag{26}$$

and

$$\Delta P=\begin{cases}-1+\cos[2\pi(f\xi)\tau] & \text{if } X<0\\ 1-\cos[2\pi(f\xi)\tau] & \text{if } X>0.\end{cases} \tag{27}$$

Here, Re is the Reynolds number, and the characteristic time ξ is defined as L/v_m. According to Eq. (12), the dimensionless frequency $f\xi$ in Eq. (27) should be 1.

The performance of the unit RED cell is of particular interest to the current study, and thus normalized representation of the short circuit current is quite helpful. In line with this, Eqs. (20) and (21) are simply rewritten to

$$I_{SC}=\frac{i_{SC}}{c_0 A}=-\frac{FD_M}{W_M}\frac{\int_A \Delta C dA}{A}, \tag{28}$$

$$\Phi_{OC}=\alpha\frac{RT}{\Lambda F}\ln\left(\frac{C_H}{C_L}\right). \tag{29}$$

The permselectivity α is set equal to 1 in this investigation.

COMPUTATIONS

For solving a set of the partial differential equations with the associated boundary conditions, Eqs. (22)-(26), an orthogonal collocation on finite element method (OCFEM) has been employed in Mathematica® (Wolfram Research Inc., IL) environment. In such a solution scheme, each channel width ($-1<X<0$ or $0<X<1$) is respectively divided into three evenly-spaced finite elements. Eleven internal collocation points are located at the zeros of the Legendre polynomial of eleventh-order defined on each finite element, thus unevenly-spaced, symmetric to center of element. Total collocation points in each finite element are thirteen, including two points placed at both ends. The collocation points along the channel length ($0<Z<1$) are defined in the same way described above.

The computational nodes on each domain (sea water and fresh water) are formed by combinations of two internal points, one from transverse direction X and the other from streamwise direction Z. Therefore, the total number of the nodes used in this study is 2,178 (=11×11×9×2). The points at each edge are determined by the boundary conditions. Computational details of this method are already addressed in many literatures [11,12]. It is worth noting that, according to experience (not shown) and other literature [3], OCFEM with 2,178 nodes provides much more stable solution than that obtained by using a finite difference method (FDM) with 9,702 nodes (=49×99×2) for this problem. In the OCFEM, the total numbers of collocation points (13 in this case) are involved for approximating first- or second-derivatives of the relevant function, while the FDM uses only two or three. The integration with respect to time is done using the built-in algorithm, NDSolve.

The values of the channel geometry, the transport properties and the subsequent dimensionless parameters are summarized in Table 1. In this study, the diffusivity variations with respect to the concentration are set very weak, assuming $\delta=1$.

Table 1. Values used in the computations of concentration and velocity profiles in RED cell

Parameters	Values	Parameters	Values
B [cm]	0.2	ρ [g/cm^3]	1
L [cm]	20	μ [g/cm·s]	0.01
W_M [cm]	0.01	p_{max} [mbar]	0.012, 0.12, 1.2
D_H [cm^2/s]	1.33×10^{-5}	Re [-]	2, 10, 20
D_L [cm^2/s]	1.33×10^{-5}	δ [-]	1
D_M [cm^2/s]	2.35×10^{-7}	β [-]	0.283
$K_H=K_L$ [-]	0.1	ξ [s]	200, 40, 20

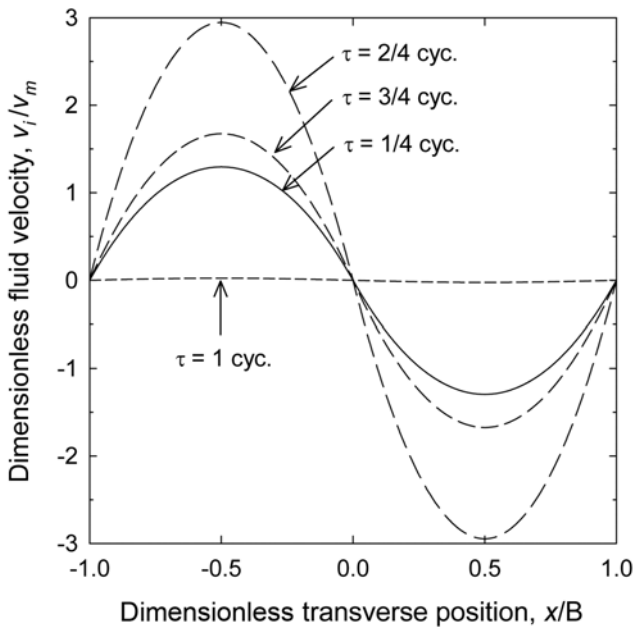

Fig. 3. Time course of velocity profiles in one cycle of pulsatile flows.

RESULTS AND DISCUSSION

The flow-rate based velocities employed in the previous experimental study with the RED unit were in the range from 0.13 to 1.2 cm/s [14]. For the comparison with these experimental results, the simulation was performed with v_m equal to 0.1, 0.5 and 1.0 cm/s. In those setups, individual Re numbers correspond to 2, 10 and 20, respectively. For further details, consult Table 1. By virtue of the time-periodic pressure gradient, Eq. (27), the velocity profiles formed across both channels are also time-periodic. Considering the dimensionless frequency $f\xi$ of 1, the entire liquid in the narrow channel is supposed to be replenished every cycle (e.g., $0<\tau<1$). For example, the first cycle of the pulsatile flow calculated with Re of 20 is drawn in Fig. 3. The velocity profile at $\tau=0.5$ is thought to show the maximum in magnitude. At $\tau=0.25$ and 0.75, the profiles represent accelerating and decelerating motions, respectively. It is noticeable that the velocity profiles at $\tau=0.25$ and 0.75 are not the same even though the pressure gradients at those times are so. It looks as though there was a time lag between pressure and velocity variations. This discrepancy is due to the inertia (i.e., Re=20) of the liquid so that it will be greater with higher Re. In addition, with much higher Re, even a non-parabolic evolution of the velocity profile can be observed [15,16].

The concentration distributions with the pulsatile flows are shown in Fig. 4, where Re is 2. The abscissa denotes the widths of two adjunct channels, and the ordinate lies along the channels. White dotted line at x/B=0 indicates the semi-impermeable membrane, in which the thickness is ignored as mentioned before. Since the velocity of the liquid is maximum at the center of each channel, the concentration of salt in the sea water side (on the left) increases fastest at the center, as shown in Fig. 4(a). After the first period ($\tau\geq1$) in Figs. 4(b) and 4(c), Na^+ is found everywhere in the sea water side. This feature results from the fact that convectional transport is dominant along the center and the entrance, while lateral diffusion is dominant near the corners at the exit. Within two periods ($\tau<2$), the entire wall x/B=−1 is covered with saline of its maximum concentration c_0 (Fig. 4(d)). In the mean time, salt continuously spreads out the fresh water channel.

Turning to the practical aspect of this simulation work, the results have been used to estimate the outstanding properties of the designed RED unit (open circuit voltage and closed circuit current), and they are compared with the values obtained from the performance tests

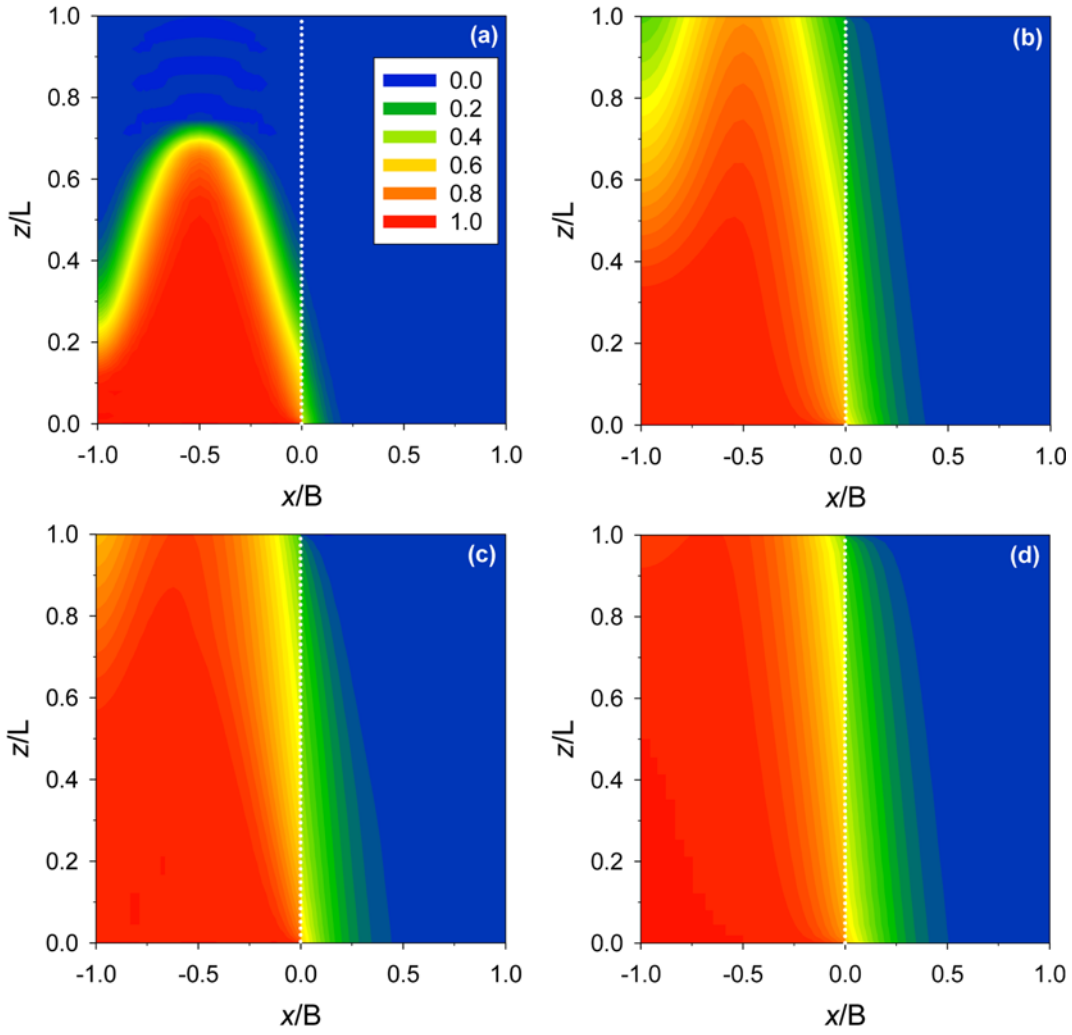

Fig. 4. Ion concentration distributions for dimensionless time τ of (a) 0.5, (b) 1.0, (c) 1.5, and (d) 2.0 formed by countercurrent pulsatile flows.

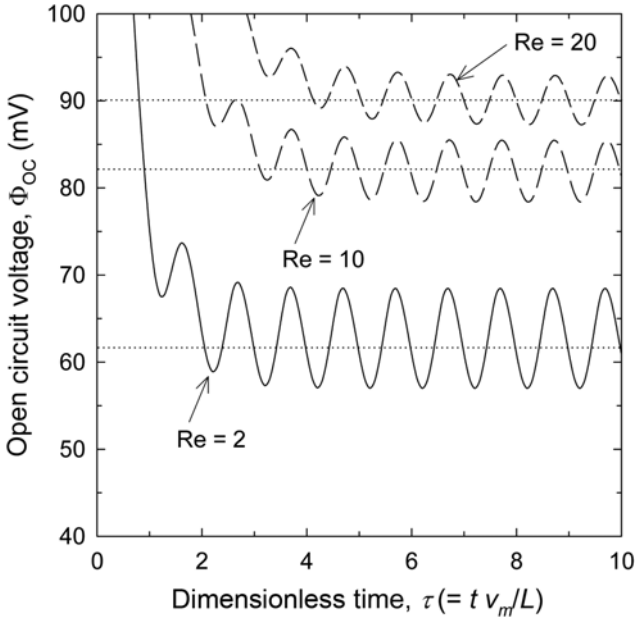

Fig. 5. The open circuit voltage Φ_{oc} of RED unit that is operated with pulsatile flows.

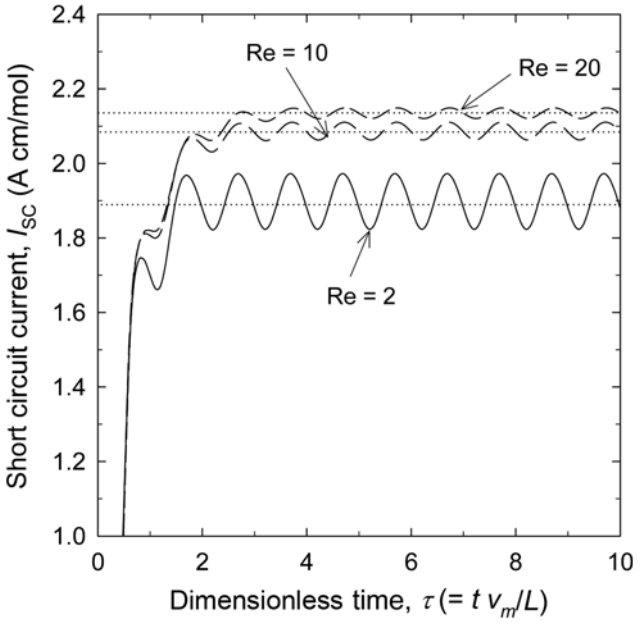

Fig. 6. The short circuit current I_{sc} of RED unit that is operated with pulsatile flows.

reported in the literature [14]. Above all, the open circuit voltages and the closed circuit currents are presented in Figs. 5 and 6, respectively. The pulsatile flow causes oscillating behaviors of the open circuit voltage and the closed circuit current. The horizontal dotted lines denote the average values of the steady oscillations. Since the concentration difference between the two channels is initially large and decreases as time elapses, the open circuit voltages are high at the beginning and then decrease to average values, i.e., 63, 82, and 90 mV for Re=2, 10 and 20, respectively. The amplitude of the oscillating voltage is around 12 mV for Re=2; it decreases with increasing Re (Fig. 5). With a steady flow, the voltage is exactly the same as the average value (not shown). This average quantity agrees with the experimental results reported by Turek et al. [14]. In practice, due to turbulence formed by the introduction of pulsatile flow in the RED unit, it is expected that average values of the oscillating open circuit voltage and closed circuit current are higher than those obtained in a steady flow system. The turbulence helps Na^+ ions mixing throughout the channel, and results in higher Na^+ concentration at the membrane surface contacting the sea water than that obtained in the steady flow. The current model, however, does not take such effect into consideration.

As a result of the pulsatile flow, the short circuit current similarly shows oscillations (averages of 1.91, 2.09, and 2.13 A cm/mol for Re=2, 10, and 20, respectively). The RED system treated by Turek [14] has the channel width of 0.019 cm and the fluid velocity ranges from 0.13 to 1.2 cm/s. Using these conditions, Reynolds numbers are given from 0.247 to 2.28. For direct comparison, the average short circuit current generated with Re=2 in our system is converted into the current density used in the experiment (A/m^2). It has 11.5 A/m^2 when the concentration of the sea water equals to 35 g/L. Therefore, it can be said that the simulation in this study provides a good approximation of the RED performance. In this calculation, the sea water is assumed to consist of only Na^+ and Cl^-. Since their atomic weights are 23 and 35 g/mol, the molarity of Na^+ is 0.603 M. Thus, the current density used in the experiments can be obtained by multiplying the conversion factor 6.03 to the results of the simulations.

CONCLUSIONS

A mathematical model describing the transport of salt by combined mechanisms of convection and diffusion has been established. The N-S equation of motion and Fickian diffusion are involved in this model, and the convective motion is induced by a pulsatile flow. The transport of salt ion through the semi-permeable membrane is implemented to set up suitable boundary conditions at the wall. The partial differential equations are numerically solved by using the orthogonal collocation on finite element method. According to the comparison with the experimental results in the literature, our numerical framework is able to provide good estimations for the open circuit voltage and the short circuit current of the RED cell. Therefore, the framework established in this study allows applying to other systems, for example, high Re number flow situations. Further, it will be useful for designing the enhanced RED system.

ACKNOWLEDGEMENT

This work was supported by the New & Renewable Energy Technology Development Program of the Korea Institute of Energy Technology Evaluation and Planning (KETEP) grant funded by the Korea government Ministry of Knowledge Economy (No. 20103020070060).

NOMENCLATURES

A : surface area of membrane [cm^2]
B : channel width [cm]

C_i : dimensionless concentration of salt [-]
c_i : concentration of salt [g/L]
D_i : diffusivity of salt [cm^2/s]
F : Faraday constant [C/mol]
f : frequency of pressure imposed to liquid in channels [s^{-1}]
I : electric current divided by salt concentration and surface area [A cm/mol]
i : electric current [A]
K_i : partition coefficient [-]
L : channel length [cm]
p : pressure [Pa]
R : gas constant [J/mol K]
Re : Reynolds number [-]
T : absolute temperature [K]
t : time [s]
V_i : dimensionless velocity of liquid in channels [-]
v_i : velocity of liquid in channels [cm/s]
v_m : average velocity of liquid based on average flow rate [cm/s]
W_M : membrane thickness [cm]
X : dimensionless transverse coordinate [-]
x : transverse coordinate [cm]
Z : dimensionless streamwise coordinate [-]
z : streamwise coordinate [cm]

Superscripts
+ : approaching to membrane from fresh water side
– : approaching to membrane from sea water side

Subscripts
H : sea water
L : fresh water
M : membrane
OC : open circuit
SC : short circuit

Greek Letters
α : efficiency factor [-]
δ : Na^+ diffusivity ratio between fresh water and sea water [-]
Λ : valence [-]
Γ : dimensionless diffusivity [-]
μ : viscosity of water [g/cm s]
ξ : characteristic time, L/v_m [s]
ρ : density of water [g/cm^3]
τ : dimensionless time [-]
Φ : voltage [V]

REFERENCES

1. R. E. Pattle, *Nature*, **174**, 660 (1954).
2. R. E. Pattle, *Chem. Proc. Eng.*, **35**, 351 (1955).
3. J. Weinstein and B. Leitz, *Science*, **191**, 557 (1976).
4. R. E. Lacey, *Ocean Eng.*, **7**, 1 (1980).
5. J. Veerman, M. Saakes, S. J. Metz and G. J. Harmsen, *J. Membr. Sci.*, **327**, 136 (2009).
6. P. E. Dlugolecki, *Mass transport in reverse electrodialysis for sustainable energy generation*, PhD Thesis, University of Twente, The Netherlands (2009).
7. J. H. Masliyah and S. Bhattacharjee, *Electrokinetic and colloid transport phenomena*, Wiley, Hoboken (2006).
8. E. L. Cussler, *Diffusion: Mass transfer in fluid systems*, 3rd Ed., Cambridge University Press, New York (2009).
9. B. S. Pivovar, Y. Wang and E. L. Cussler, *J. Membr. Sci.*, **154**, 155 (1999).
10. Y. Jeong and I. S. Kang, *Korean J. Chem. Eng.*, **12**, 540 (1995).
11. K. S. Kim and L. Simon, *Comput. Chem. Eng.*, **35**, 1152 (2011).
12. K. S. Kim and L. Simon, *Math. Biosci.*, **229**, 93 (2011).
13. B. A. Finlayson, *Nonlinear analysis in chemical engineering*, McGraw-Hill, New York (1980).
14. M. Turek and B. Bandura, *Desalination*, **205**, 67 (2007).
15. P. Goswami and S. Chakraborty, *Langmuir*, **26**, 581 (2010).
16. S. Vedel, L. H. Olesen and H. Bruus, *J. Micromech. Microeng.*, **20**, 035026 (2010).